

# A portable, robust, stable and tunable calibration source for gas-phase nitrous acid (HONO)

Melodie Lao<sup>1</sup>, Leigh R. Crilley<sup>1</sup>, Leyla Salehpoor<sup>1</sup>, Teles C. Furlani<sup>1</sup>, Ilann Bourgeois<sup>2,3</sup>, J. Andrew Neuman<sup>2,3</sup>, Andrew W. Rollins<sup>2</sup>, Patrick R. Veres<sup>2</sup>, Rebecca A. Washenfelder<sup>2</sup>, Caroline C. Womack<sup>2,3</sup>, Cora J. Young<sup>1</sup>, and Trevor C. VandenBoer<sup>1,\*</sup>

<sup>1</sup> Department of Chemistry, York University, Toronto, ON

<sup>2</sup> NOAA Chemical Sciences Laboratory, Boulder, CO

<sup>3</sup> Cooperative Institute for Research in Environmental Sciences, University of Colorado, Boulder, CO

\* Communicating Author: [tvandenb@yorku.ca](mailto:tvandenb@yorku.ca)

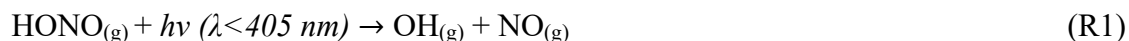
## Abstract

Atmospheric HONO mixing ratios in indoor and outdoor environments span a range of less than a few parts per trillion by volume (pptv) up to tens of parts per billion by volume (ppbv) in combustion plumes. Previous HONO calibration sources have utilized proton transfer acid displacement from nitrite salts or solutions, with output that ranges from tens to thousands of ppbv. Instrument calibrations have thus required large dilution flows to obtain atmospherically relevant mixing ratios. Here we present a simple universal source to reach very low HONO calibration mixing ratios using a nitrite-coated reaction device with the addition of humid air and/or HCl from a permeation device. The calibration source developed in this work can generate HONO across the atmospherically relevant range and has high purity (>90 %), reproducibility, and tunability. Mixing ratios at the tens of pptv level are easily reached with reasonable dilution flows. The calibration source can be assembled to start producing stable HONO mixing ratios (RSE  $\leq$  2 %) within two hours, with output concentrations varying  $\leq$  25 % following simulated transport or complete disassembly of the instrument, and  $\leq$  10 % under ideal conditions. The simplicity of this source makes it highly versatile for field and lab experiments. The platform facilitates a new level of accuracy in established instrumentation, as well as intercomparison studies to identify systematic HONO measurement bias and interferences.

## 1. Introduction

In the lower troposphere, the hydroxyl radical (OH) is the principal daytime gas-phase oxidant, and will react with volatile organic compounds (VOC) to form secondary pollutants such as ozone (O<sub>3</sub>) and secondary organic aerosols (Spataro and Ianniello, 2014; Ye et al., 2018). Photolysis of nitrous acid (HONO) is a direct source of the hydroxyl radical (OH) (R1). Consequently, this can be a significant contributor to the integrated daily OH budget, ranging from 4-56 % in urban areas (Lee et al., 2013; Volkamer et al., 2010), up to 80% in semi-rural areas in the winter (Kim et al.,

2014), along with additional vertical and temporal variability (Crilley et al., 2016; Young et al., 2012; Zhang et al., 2009).



40 The reported daytime mixing ratios of ambient HONO outdoors can vary considerably for different environments, ranging from a few parts per trillion by volume (pptv) in the clean remote marine and Arctic boundary layers (Honrath et al., 2002; Kasibhatla et al., 2018; Reed et al., 2017) to 18 parts per billion by volume (ppbv) in polluted megacities such as Milan, Los Angeles, and Beijing (Elshorbany et al., 2009; Febo et al., 1996; Harris et al., 1982; Tong et al., 2016; Zhang et al., 45 2019). Measurements within biomass burning plumes from forest fires have shown very high HONO levels, often up to 60 ppbv (Chai et al., 2019; Neuman et al., 2016; Veres et al., 2010b). There is a growing body of evidence that HONO concentrations can be significant in indoor environments, with levels up to 50 ppbv reported from gas stove cooking emissions (Collins et al., 2018; Gligorovski, 2016; Gómez Alvarez et al., 2012; Liu et al., 2019; Young et al., 2019; Zhou 50 et al., 2018). There are a number of atmospheric HONO sources that have been reported: direct emissions (e.g. vehicles and biomass burning); gas-phase homogenous reaction of NO and OH, biological production in soils (Mushinski et al., 2019), and a number of heterogeneous surface reactions ((Spataro and Ianniello, 2014) and references therein). Despite the importance of HONO to atmospheric photochemistry and radical budgets, the contribution of these sources to observed 55 HONO levels is still poorly constrained, particularly during the daytime (Gall et al., 2016; Kleffmann, 2007; Lee et al., 2016; Oswald et al., 2013; Pusede et al., 2015; Sörgel et al., 2015; Tsai et al., 2018; Ye et al., 2016).

Due to the importance of HONO in our understanding of tropospheric photochemical oxidation and indoor atmospheric oxidation chemistry, accurate and precise quantitative measurements are 60 required. However, gas-phase HONO has remained a challenging compound to measure due to several instrument artefacts and interferences. Within inlet lines, positive artefacts can occur as a result of heterogenous HONO formation on wet surfaces (Kleffmann and Wiesen, 2008; Zhou et al., 2002), while the reactive nature of HONO can also lead to negative artefacts due to wall losses (Pinto et al., 2014). Furthermore, there can be interferences from ambient components in the 65 atmospheric matrix, such as the reduction of NO<sub>2</sub> by numerous compounds, as well as particulate nitrite (Kleffmann et al., 2006; Kleffmann and Wiesen, 2008; Rubio et al., 2009; Sörgel et al., 2011; VandenBoer et al., 2014). Recent intercomparison studies have shown substantial differences between various HONO measurement techniques (Cheng et al., 2013; Crilley et al., 2019; Pinto et al., 2014; Stutz et al., 2010). Crilley et al. (2019) observed that while different 70 HONO measurement techniques agreed on the temporal trends in HONO concentrations, the reported absolute concentrations displayed systematic variation. Most studies are unable to pinpoint the exact cause of the observed divergence between instruments; it may be due to spatial heterogeneity in ambient HONO concentration, unknown chemical interference(s), and/or differences in the accuracy and precision of calibration approaches. A portable calibration unit

75 compatible with all instruments/techniques could assist in ruling out systematic bias and  
identifying interferences between instruments during intercomparison studies.

A variety of approaches have been used in the past to generate gaseous HONO standards. Most of  
these depend on acid displacement from a solution containing nitrite ( $\text{NO}_2^-$ ) or from solid sodium  
nitrite ( $\text{NaNO}_2$ ). Acids used have included sulfuric acid, hydrochloric acid, and oxalic acid, with  
80 evaporation of  $\text{NH}_4\text{NO}_2$  also reported (Braman and de la Cantera, 1986; Febo et al., 1995; Taira  
and Kanda, 1990; Večeřa and Dasgupta, 1991). By far the most widely employed modern HONO  
calibration methods stem from the report of Febo et al. (1995) who presented a system for  
generating a continuous source of stable gas-phase HONO in the tens of ppbv to parts per million  
by volume (ppmv) range. This system utilised the reaction between gas-phase hydrochloric acid  
85 ( $\text{HCl}$ ) and  $\text{NaNO}_2$  powder to generate gas-phase HONO, as described in R2:



However, this calibration source requires a gas-tight vessel of  $\text{HCl}$  solution contained in a  
thermostatic bath that presents considerable difficulty for many field measurement applications.  
Adaptations include immersing thin-wall Teflon tubing in concentrated  $\text{HCl}$ , high concentration  
90  $\text{HCl}$  cylinders, and  $\text{HCl}$  permeation devices. Gaseous  $\text{HCl}$  generated by these methods then mixes  
with loose  $\text{NaNO}_2$  crystals in a stirred reactor (Stutz et al., 2000), dispersed using 3 mm glass  
beads packed in PFA tubing to increase porosity (Roberts et al., 2010), or pieces of PFA tubing  
(McGrath et al., 2019; VandenBoer et al., 2015; Zhou et al., 2018). These adapted approaches have  
been used to calibrate many atmospheric HONO instruments (Crilley et al., 2019; Heland et al.,  
95 2001; Ren et al., 2010; Roberts et al., 2010; Stutz et al., 2000; VandenBoer et al., 2013, 2015;  
Wang and Zhang, 2000; Young et al., 2012). An alternative approach that utilised dilute  $\text{H}_2\text{SO}_4$   
for the acid displacement reaction with aqueous  $\text{NaNO}_2$  was outlined by Taira and Kanda (1990).  
While this approach was shown to generate a stable and tunable HONO output at hundreds of  
ppbv, it has not been widely adapted, likely due to the need for complex custom glassware and  
100 liquid flow control in the calibration apparatus and significant dilution to reach single digit ppbv  
mixing ratios (Kleffmann et al., 2004).

While widely used, the method described by Febo et al. (1995) presents several practical  
challenges. The typically high HONO mixing ratios generated by this approach (up to 20 ppmv)  
are challenging to dilute to atmospherically relevant mixing ratios. The high quantities also lead  
105 to auto-dissociation of HONO (R3), resulting in the production of nitrogen oxide impurities of  $\text{NO}$   
and  $\text{NO}_2$  (Febo et al., 1995; Neuman et al., 2016), and  $\text{ClNO}$  in the presence of  $\text{HCl}$  at ppmv levels  
(Gingerysty and Osthoff, 2020).



Further, to reduce the variability in HONO output over time, the powdered  $\text{NaNO}_2$  bed requires  
110 continuous mixing to maintain equilibrium between the adsorbed HONO and carrier gas flowing  
over the salt bed minimize the production of  $\text{NO}_x$  by R3, as well as a Teflon filter to prevent loss

of  $\text{NaNO}_2$  powder by entrainment in the gas flow. The degradation of the powdered  $\text{NaNO}_2$  structure can limit the lifetime of the source and results in unstable HONO production rates (Febo et al., 1995; Gingerysty and Osthoff, 2020). Other systems using dispersed  $\text{NaNO}_2$  suffer from sensitivity to vibration, causing changes in HONO output and limiting calibration accuracy (Zhou et al., 2018). Once operational, the original or modified methods require up to a day to stabilize and these systems must be kept continuously operating and stationary to preserve the HONO output stability.

One solution for producing gaseous HCl for acid displacement is to use a temperature-controlled permeation device (PD). A permeation oven is a simple instrument that can be used for the preparation of low mixing ratios of gases from ppbv to ppmv levels (Veres et al., 2010a; Washenfelder et al., 2003). This approach has been used to generate a consistent quantity of gaseous analytes for over 400 compounds because it is low-cost, portable, and robust (Mitchell, 2000). Permeation devices are typically made of inert polymer tube of known permeability filled with a (semi-)volatile liquid. Both ends of the device are sealed either with caps or permeable plugs and the emission is determined by the surface area and thickness of permeable polymer, the concentration of the contained solution, and the temperature (O’Keeffe and Ortman, 1966; Susaya et al., 2012).

The aim of the current work was to make a portable and easy to assemble HONO calibration instrument compatible with HONO-measuring instruments commonly used within the atmospheric research community. We developed coated devices to facilitate reactions of sodium nitrite ( $\text{NaNO}_2$ ) which release HONO when exposed to water vapour and HCl (R2). Herein we demonstrate that the  $\text{NaNO}_2$ -coated reaction devices produce a stable and continuous supply of high-purity gaseous HONO. The output of this HONO calibration source spans the range of environmentally relevant mixing ratios, up to tens of ppbv. The emission quantities, mass balance, and purity of gaseous HONO were determined through a series of control tests with various instruments. We present evidence of its robustness, reproducibility, and stability in HONO output. Finally, we evaluated methods to control the mixing ratio output of the calibration source and provide several approaches and recommendations on its use.

140

## 2. Experimental Methods

### 2.1 Coated $\text{NaNO}_2$ reaction devices

Reactions of  $\text{NaNO}_2$  on humidified surfaces produce HONO. A large and consistent surface area is required to reproducibly produce HONO at the desired levels.

145 A  $\text{NaNO}_2$  (EMSURE®; ACS Reag. Ph Eur, Germany) coating solution was made as a  $20 \text{ g L}^{-1}$   $\text{NaNO}_2$  solution. The coating solution solvent was composed of equal volumes of methanol (HPLC Grade; Fisher Chemicals, Ottawa, ON) and  $18.2 \text{ M}\Omega\cdot\text{cm}$  deionised water with  $1.0 \text{ g L}^{-1}$  glycerol

(Sigma Chemical Company, St. Louis, MO, USA) to facilitate a uniform salt coating. The solution was made by dissolving the  $\text{NaNO}_2$  in the water first, followed by the addition of the glycerol and then methanol. The coating solution was stored in an HDPE bottle wrapped in aluminum foil at 4 °C until needed and remade every three months. To coat a reaction device, 3 mL of coating solution was first transferred into a heat-straightened  $\frac{1}{2}$ " (1.27 cm) PFA tube with a length of 14.4 cm and surface area of 86.2  $\text{cm}^2$ . Rubber stoppers with centred 4.5 mm holes were inserted into both ends of the PFA tube to reduce solution loss while evaporating the solvent. The PFA reaction device was repeatedly inverted and rotated while covering both stopper holes to coat the inner surface completely. The reaction device was then dried by insertion into an 8" (20 cm) length of aluminum pipe (1- $\frac{1}{4}$ "/3.18 cm I.D.) and placed onto heated stainless steel rollers to evenly coat the PFA reaction device surface as the solution evaporates over a few hours (Nostalgia Electrics, RHD800 Retro Series; or Great Northern Popcorn Company, 4078 GNP Hotdog 7 Roller Machine). Until their experimental use, prepared  $\text{NaNO}_2$  PFA reaction devices were sealed with Parafilm or vinyl end caps (McMaster-Carr; P/N: 40005K14) and kept in a dark box at room temperature.

Teflon-coated aluminum annular denuders (URG-2000-30x150-3CSS, URG Corporation, Chapel Hill, NC) were also used in some experiments in place of the  $\text{NaNO}_2$  device (Figure 1). To coat these denuders, 3.0 mL of the  $\text{NaNO}_2$  coating solution was transferred to the device, followed by capping, inversion, rotation and shaking to ensure all concentric etched glass surfaces were coated. The excess  $\text{NaNO}_2$  coating was decanted and the denuder dried with zero air at a flow of 1.0 standard litre per minute (SLPM) for about 10 min at room temperature.

## 2.2 Gas flows

The calibration source, which uses a permeation oven and  $\text{NaNO}_2$  reaction device to generate HONO, was designed to be cost-effective, lightweight, and robust for use with dry compressed air as the carrier gas (Figure 1). Full technical details of the design rationale and assembly of the custom-built permeation oven can be found in the Supporting Information (SI, Sections S1-2, Figures S1-5), with only a brief description given below. A  $\text{NO}_x$  analyzer was used to characterize the output from the HONO source. A single cylinder or zero air generator provided the separate carrier gas flows required for the PD, a humidifier, and a dilution flow.

Carrier gas flow through the permeation oven was provided by a compressed cylinder of zero air or nitrogen (Praxair; Air Ultra Zero, 99.999%, AI 0.0UZ-K; High Purity Nitrogen, 99.998 %, NI 4.8, Toronto, ON) but an in-situ zero air generator could also be used (e.g. Aadco Instruments Model 747-10, Cleves, OH; used only for dilution flows here) providing 20 psi of pressure to control the flow entering a four-way  $\frac{1}{4}$ " (64 mm) Swagelok cross fitting. The zero air flows through two critical orifices setting flows of  $\sim 50$  sccm (Lenox Laser, Glen Arm, MD; SS-4-VCR-2-50) and a mass flow controller (MFC; MKS Instruments, Inc.; M100B00814CS1BV, 10 SLPM, gas; AIR, Kanata, Canada) set to deliver a dilution flow of 1.0 SLPM. A proportional-integral-differential (PID) temperature controller (Omega™; CN 7823, St-Eustache, QC) was used to regulate the temperature of a machined aluminum (Al) block. The first critical orifice connects to

the HCl PD channel within the heated Al block and the second connects to a 25 mL glass impinger (EMD Millipore Corporation, Billerica, MA, USA) containing deionised water at room temperature. The flows are combined and mixed to a resultant relative humidity (RH) of 50 %, which then enters the coated NaNO<sub>2</sub> reaction device in the temperature-controlled Al block. The HCl drives the acid displacement reaction in the NaNO<sub>2</sub>-coated PFA device, releasing HONO into the gas phase. The flow exits the oven into the dilution flow being delivered to an instrument or experimental system. If operating in cold environments, care should be taken to ensure the 50 % RH exiting the calibration system does not generated condensation in the lines.

### 2.3 Custom-built HCl permeation devices (PDs)

Although PDs are available from commercial suppliers, they are custom made here to reduce costs, as described in detail in the Supporting Information (Section S2, Figure S5). Briefly, custom PDs are made from PFA tubing (3.2 mm ID with 5 mm OD, P/N: 5733K73; McMaster-Carr, Aurora, OH) fitted with PTFE plugs (3.2 mm diameter, P/N: 84935K64; McMaster-Carr). A series of HCl PDs were made as aqueous solutions to obtain PDs containing 1.2 M and 6 M HCl solutions (OmniTrace®; 34-37 %, HX0607-1, SigmaAldrich, Oakville, ON; Table 1). During operation the HCl PD is placed within the ½” tubing in the heating block, through which the carrier gas is flushed.

### 2.4 NO<sub>x</sub> analyzer for HONO detection

The output from the HONO calibration source was monitored using a commercial chemiluminescent NO<sub>x</sub> analyzer fitted with a Mo catalytic converter, set to 325 °C (Serinus 40, American Ecotech, Warren, RI). The conversion efficiency of NO<sub>2</sub> to NO was calculated by combining known concentrations of NO from a standard cylinder (Praxair; NI NO5MC-A3, 4.88 (±5 %) ppmv, Toronto, ON) and O<sub>3</sub> using a gas calibration instrument (Gascal 1100TS, American Ecotech, Warren, RI). The conversion efficiency was determined according to the manufacturer specifications at 98.84 (±0.38 %) for NO<sub>2</sub> mixing ratios delivered to the system spanning 100 to 400 ppbv. While the Mo catalyst is meant to convert NO<sub>2</sub> to NO for detection by the analyzer, it is well known that HONO is also quantitatively converted to NO (Febo et al., 1995), and the conversion efficiency was determined experimentally (Section 2.6). A NO<sub>x</sub> analyzer was preferred to other independent calibration methods such as ion chromatography with conductivity detection (IC-CD), as it is capable of continuous real-time measurement of HONO, allowing rapid frequent checks on the calibration source output stability.

During experiments, ~100 sccm from the HONO source was diluted into an additional 1.0 SLPM of zero air from which the NO<sub>x</sub> instrument sampled 0.63 SLPM (Fig. 1). The NO<sub>x</sub> analyzer measured NO on either the NO or NO<sub>x</sub> channels for an averaging period of 1 minute with the Kalman filter set to 60 s or 300 s. To correct for instrument drift or NO<sub>x</sub> contamination in the zero air, the analyzer was flushed for at least 15 min at the beginning and end of each experiment. An annular denuder coated with 20 g L<sup>-1</sup> sodium carbonate in 50:50 methanol and water solution

(Na<sub>2</sub>CO<sub>3</sub>; ACS reagent >99.7%; SigmaAldrich, St. Louis, MO) – similar to that used here for NaNO<sub>2</sub> - was inserted during some experiments to scrub HONO from the experimental flow (Fig. 1). The denuder was prepared by transferring 10 mL of Na<sub>2</sub>CO<sub>3</sub>-coating solution, capping, then inverting and rotating to distribute the solution evenly. The remainder of the coating solution was decanted and the denuder surfaces dried under a flow of 1.0 SLPM of zero air until completely dry (~10 min). The denuder was inserted into experimental flows for at least one hour as a second check on sources of background NO and NO<sub>2</sub> as impurities being emitted from the calibration source or carrier gas. A Na<sub>2</sub>CO<sub>3</sub> denuder can also be used as a robust alternative to provide the NO<sub>x</sub> analyzer inlet overflow instead of a cylinder of zero air. This enables corrections of HONO measurements or calibrations for NO<sub>x</sub> present in the sample air or calibration source carrier gas, respectively.

## 2.5 Conversion efficiency of the NO<sub>x</sub> analyzer Mo-catalyst for HONO

A Mo catalyst at 325 °C will reduce HONO to NO, though reports have shown that this conversion may vary between NO<sub>x</sub> analyzers (McGrath et al., 2019; Zhou et al., 2018). We measured the HONO generated by the calibration source with the NO<sub>x</sub> analyzer, then directed the HONO to a scrubbing solution of 1 mM NaOH in two glass impingers connected in series for several hours to days to collect NO<sub>2</sub><sup>-</sup> to a level that could be quantified by IC-CD. The second bubbler was used to determine the extent that HONO was quantitatively collected in the first bubbler (i.e. to capture any breakthrough). The HONO generated by the calibration source and quantified by IC was compared to the NO<sub>x</sub> analyzer measurement, using the introduction of a Na<sub>2</sub>CO<sub>3</sub> annular denuder to perform background correction. The HONO conversion efficiency determined by comparison to the IC was found to be 104 ± 4 % (n = 3), confirming unit conversion efficiency, with the associated error set by the 4 % accuracy of the IC-CD method for NO<sub>2</sub><sup>-</sup> (R<sup>2</sup> > 0.999) when employing our previously developed separation method (Place et al., 2018). The IC precision near the analyzed concentrations for NO<sub>2</sub><sup>-</sup> was measured to be 3 %. All data presented in this manuscript therefore uses a conversion efficiency of unity for the Mo-catalyst.

## 2.6 Supporting Instrumentation

In our mass balance experiments for the production mechanisms governing HONO generation in the calibration system, we used two additional tools to monitor experimental gas flows. Mixing ratios of HCl were measured at 0.5 Hz using a cavity ring down spectrometer (CRDS) (G2108 HCl Gas Concentration Analyzer, Picarro, Santa Clara, CA) with a 5 pptv detection limit for 1-minute averaged data. Further details on the performance of this instrumentation can be found in Dawe et al. (2019). Measurements of HCl and HONO to investigate acid displacement efficiency of the calibration system were measured at 2 Hz using a quadrupole chemical ionisation mass spectrometer (CIMS, THS Instruments LLC, Atlanta, GA) using acetate reagent ions to facilitate proton transfer and detection of negative ions at m/z 35 and 46, respectively. Observed ions were normalized to the detected quantity of the acetate reagent ion and multiplied by 8x10<sup>5</sup>, resulting in signal units of normalized counts, as we have previously reported for the detection of these analytes

(VandenBoer et al., 2013). Signal from the CIMS was averaged to a 1-minute time base to compare to other measurements.

In our purity and stability experiments, additional instrumentation was used to detect HONO, NO<sub>y</sub>, and other reactive gases. A time-of-flight chemical ionisation mass spectrometer utilising iodide adduct reagent ions (I<sup>-</sup> ToF-CIMS; Aerodyne Research Inc., Billerica, MA) was used to measure HONO and detect a wide array of other analytes (e.g. ClNO<sub>2</sub>, HNO<sub>3</sub>, N<sub>2</sub>O<sub>5</sub>, etc.) in experimental gas flows. Specific operational details of the I<sup>-</sup> ToF-CIMS for these atmospheric species are presented elsewhere (Neuman et al., 2016; Veres et al., 2020). A broadband cavity enhanced absorption spectrometer (ACES) was used to measure HONO and NO<sub>2</sub> (Min et al., 2016) and a single-photon laser induced fluorescence (LIF) instrument was used to measure NO (Rollins et al., 2020). A high sensitivity chemiluminescent NO instrument fitted with a gold catalyst (NO<sub>y</sub>O<sub>3</sub>) was used to quantify NO and NO<sub>y</sub> (Fahey et al., 1985; Fontijn et al., 1970; Ridley and Grahek, 1990; Ridley and Howlett, 1974; Ryerson et al., 1999).

### 275 **3 HONO calibration source characterization**

#### **3.1 NaNO<sub>2</sub>-coated reaction device**

Previous calibration methods required a 1-2 g bed of loose crystalline NaNO<sub>2</sub> to generate high mixing ratios of HONO, but only consumed a minimal amount of NaNO<sub>2</sub> from the total supply before being thrown away (Febo et al., 1995; Roberts et al., 2010). At maximum, our NaNO<sub>2</sub> coated PFA reaction devices could contain up to 60 mg of NaNO<sub>2</sub> (3.0 mL x 20 g L<sup>-1</sup> NaNO<sub>2</sub> coating solution) or 40 mg of NO<sub>2</sub><sup>-</sup> if there was 100 % coating efficiency. Due to the hydrophobic nature of PFA and the loss of liquid solution from the drying procedure, however, the reaction device retained only a fraction of the applied NaNO<sub>2</sub>. The amount of NO<sub>2</sub><sup>-</sup> present after coating the PFA devices (n = 3) was determined by rinsing with deionised water and analysis by IC-CD. An average mass of 0.53±0.27 mg NO<sub>2</sub><sup>-</sup> was deposited on the surface of the PFA device, 1.3 % of the total NO<sub>2</sub><sup>-</sup> applied. The quantity coated on the PFA devices was sufficient to generate stable, low mixing ratios of HONO for extended periods. To efficiently use most of the salt, we calculated how long the NaNO<sub>2</sub> coating could provide a specific calibration mixing ratio of HONO (E1). Thus, we designed and operated our coated devices based on their calculated capacity to generate a specific mixing ratio of HONO (C<sub>HONO</sub>) continuously over time based on the number of moles of NaNO<sub>2</sub> deposited in the coating (n<sub>NaNO2</sub>) and the total dilution flow in moles of air for that same duration (F<sub>air</sub>).

$$C_{\text{HONO}} = n_{\text{NaNO}_2} / F_{\text{air}} \quad (\text{E1})$$

To generate higher mixing ratios of HONO, more NaNO<sub>2</sub> mass and/or coated surface area are required. The higher surface area of a coated glass annular denuder housed in Teflon-coated aluminum tubing was explored for use as an alternative to PFA tubing. To test this, three annular denuders were prepared using the same volume of coating solution. An average mass of 7.26±1.80



300 mg of  $\text{NaNO}_2$  on the denuder surface was determined, 18 % of the total applied. Thus, the coated annular denuder resulted in about eighteen times more deposited  $\text{NaNO}_2$  than the PFA devices, due to the higher available surface area of pattern-etched glass. Unfortunately, these devices proved unstable, as discussed below, and are expensive. The HONO output from other tubing materials were also tested (Section 3.7.2).

305 The lifetime of the  $\text{NaNO}_2$  devices can be approximated using E1, under the assumption that a stable output of HONO is generated from the start of the experiment. At standard room temperature and pressure a device generating 2 ppbv of HONO and containing the average 0.53 mg of  $\text{NO}_2^-$  observed for the PFA device could last for up to 88 days. In practice, we observed a PFA device generating approximately 2 ppbv  $\text{min}^{-1}$  of HONO to be reliable for over four weeks during experiments performed to test the stability and reproducibility of the PFA devices (Sections 3.5, 310 3.6). The lifetime of the device is expected to decrease proportionally if a higher output of HONO for a given mass of  $\text{NaNO}_2$  coating is required. Decreasing HONO mixing ratios on the order of a hundred pptv on hourly timescales (for an initial few ppbv of output) was used as a metric to indicate that coated reaction devices were depleted since their output was no longer stable.

### 315 **3.2 HONO generation with water vapour**

Prior calibration sources have exclusively reported HONO production via the acid displacement mechanism. In the mass balance experiments reported below, where we employ this mechanism, it was discovered that water vapour alone was responsible for a measurable amount of the generated HONO in the ppbv regime. Mixing ratios of HONO produced using our coated PFA 320 reaction devices exposed to water vapour were too low to accurately measure using our  $\text{NO}_x$  analyzer ( $\leq 0.6$  ppbv). To explore the influence of water vapour (i.e. humid air) on HONO output, we performed a series of experiments at different RH using an  $\text{NaNO}_2$  coated annular denuder. The denuder generated higher HONO mixing ratios, on the order of several ppbv in 1.1 SLPM. Prior to the experiments, the calibration source unit was flushed with zero air for at least 12 hours. 325 The absence of  $\text{HCl}$  ( $< 5$  pptv) was confirmed with the CRDS. When the RH passing through the denuder was 0 % we observed no HONO, with signal near the detection limit of the  $\text{NO}_x$  analyzer ( $0.50 \pm 0.48$  ppbv,  $n = 43$ ). When we increased the RH of the carrier gas, we observed the production of HONO, but the variation was not monotonic. At a RH of 25 % HONO output increased to  $11.73 \pm 0.39$  ppbv ( $n = 35$ ) followed by a decrease at an RH of 50 % to  $8.60 \pm 0.63$  ppbv ( $n = 38$ ). 330 This trend is likely due to the effective Henry's Law constant of HONO in the aqueous film on the surface of the  $\text{NaNO}_2$  device, due to the weak acid nature of HONO ( $\text{pK}_a = 3.4$ ). When the humidity is higher, less HONO may be released from the surface due to the increased presence of water in which a larger equilibrium concentration of aqueous nitrite can be sustained. This contrasts with  $\text{HCl}$  ( $\text{pK}_a$  of -8), which completely dissociates in aqueous solution on the surface of 335 the  $\text{NaNO}_2$  device and facilitates the acid displacement mechanism (R2).

This is the first observation of water vapour-produced HONO. Prior calibration sources typically generated very high HONO mixing ratios from 100 ppbv up to tens of ppmv in the displacement vessel, resulting in the contribution from humid air being undetected (Febo et al., 1995; Gingerysty and Osthoff, 2020; McGrath et al., 2019; Roberts et al., 2010; VandenBoer et al., 2015; Zhou et al., 2018). The observed HONO mixing ratios from this mechanism in our experiments would likely be within error of the mass balance calculations, or indistinguishable from noise in the analytical instrumentation in prior reports. Our results suggest that the use of water vapour passed over a  $\text{NaNO}_2$  coated PFA reaction device produces sub-ppbv mixing ratios of HONO for calibration of instruments making ambient observations in remote environments. Using water vapour alone, the only way to increase the HONO mixing ratios from the calibration system is to increase the available amount of  $\text{NaNO}_2$ , which is challenging (Sections 3.1 and 3.7.2). A more controlled approach to reach higher mixing ratios is through the acid displacement technique.

### 3.3 HCl emissions from custom-built PDs

To generate stable HONO mixing ratios using an  $\text{NaNO}_2$  reaction device on the order of a few to tens of ppbv, a stable source of HCl is required. The HCl generated from custom-made PDs was therefore evaluated as a function of solution concentration contained (1.2 – 6 M), temperature (30 – 60 °C), and stability by CRDS (Table 1, Figure S6). Custom-made PDs of different concentration and lengths were tested for their ability to produce a range of HONO mixing ratios. Custom-made PDs have been previously demonstrated in our work to provide a stable emission source of HCl (MacInnis et al., 2016). The HCl output was found to be temperature-dependent and increased exponentially with temperature, as expected from theory (Section S2). However, as the PD was ramped to higher temperatures ( $> 50$  °C) the permeation rate became more unstable, with a resulting settling time of about an hour as the materials from the permeation oven apparatus re-equilibrated (Figure S7). Since the HCl PDs were observed to be most stable at 30 °C and 40 °C, these temperatures were considered optimal to generate the stable HONO mixing ratios. Note that the HONO mixing ratios in the 100 sccm flow exiting the reaction device range from 9.7 to 72 ppbv (Table 1), which are much lower than all prior calibration sources, enabling easy dilution to reach environmentally relevant HONO mixing ratios for instrument calibration or experimental applications.

Two newly made 6 M HCl PDs (-6b and -6c) were found to emit different, yet highly stable (e.g.  $\pm 0.01$  ppbv), mixing ratios at identical oven temperatures (Figure S6). This demonstrates potential variability with each new device due to inconsistent results during custom fabrication compared to commercial PDs. The most likely source of such differences in output is variability in our sealing of the PTFE plugs resulting in increased emission rates. In any case, the PDs remain stable with less than 10 % relative standard deviation. In comparison, commercial device emission rates are often certified within  $\pm 30$  %. The emission rates of commercial PDs are certified through measurement by gravimetric weight loss over time ( $\text{ng min}^{-1}$ ). A commercial  $\frac{1}{4}$ " (64 mm) Teflon HCl PDs of 6.55 M certified to emit  $1905 \pm 520$  ppbv in 100 sccm flow at 40 °C (RSD = 27.3 %;

VICI Metronics, Inc.; Poulsbo, WA), has this output variance due to the co-emission of water and propagated measurement uncertainties. A lower variance in the emitted HCl was observed from our custom-made PDs when we quantified HCl directly by either CRDS or IC-CD. Custom-built PDs were therefore chosen over commercial PDs due to their demonstrated stability and low cost. It was found that HCl outputs of the custom-PDs slowly diminished over time, which emphasizes the need for regular calibrations. For example, the HCl output from two-year-old PD-6a emitted 0.21±0.01 ppbv in 1.1 SLPM in comparison to 2.0±0.01 ppbv when it was newly made, which decreased the resulting HONO generation in the reaction device. Similar results have been observed in calibrations with PDs of aqueous NH<sub>3</sub> and HNO<sub>3</sub> solutions decreasing by ~30 % during two years of storage, as well as for carbonyl sulfide (Fried et al., 1998; Neuman et al., 2003). Despite the decreasing HCl output over a year or more of use, HCl PDs act as a stable acid source on the order of weeks, producing consistent HCl output to subsequently generate stable HONO, even when removed from the permeation oven or stored for up to two months. Overall, it is difficult to replicate PD emission rates using the same HCl concentration and material dimensions for a custom-PD. The custom-built PD seals can be altered by replacing the PTFE plug by crimping the ends of heated-to-pleiability PFA tubing to form welded polymer ends (Section S2). Such an approach is expected to improve the reproducibility of the custom-device emission rates but is beyond the scope of this work to explore in more detail.

### 3.4 Acid displacement to generate HONO

Two techniques were used to assess the reaction completion between HCl and NaNO<sub>2</sub> in the calibration system. We applied a mass balance approach that combined the CRDS measurement of HCl, our NO<sub>x</sub> analyzer HONO measurement, and IC-CD quantitation of these acids scrubbed into 1 mM NaOH. The displacement efficiency was further confirmed by simultaneous observation of HCl and HONO by acetate quadrupole CIMS.

#### 3.4.1 Mass balance of HONO generated

Experiments were conducted to confirm that HONO can be generated by introducing only humid air (50 % RH) within the NaNO<sub>2</sub> devices without the presence of HCl. In humid air, we observed HONO levels above the detection limit (DL) of the NO<sub>x</sub> analyzer. A single PFA device exposed to humid air (50 % RH) released up to 0.61 ppbv of HONO – equivalent to 77 % of the total HONO generated when coupled with an HCl PD (Table 2). The reaction of the humidified NaNO<sub>2</sub>-coated device, resulting in the release of HONO, implies formation of NaOH. Further speculation on the reaction mechanism is beyond the scope of this work. Given the existing challenge in producing low mixing ratios of HONO in the pptv range, it appears that these can be reached most easily without the use of an HCl PD in our calibration system, while higher mixing ratios necessitate the addition of HCl (Section 3.7). The NO<sub>x</sub> analyzer signal was indistinguishable from zero when the NaNO<sub>2</sub> reaction device was absent, but all other conditions were matched. This demonstrates that HONO was generated only within the NaNO<sub>2</sub> reaction device.

415 The total flow for all mass balance experiments was 1.1 SLPM (Fig. 1) with zero air flows  
replacing those typically carrying reagents when they were removed. We observed that the HONO  
output from the reaction devices was greater than the HCl input from the PDs, confirming that  
another chemical reaction was generating the remaining HONO (Table 2). Mass balance could  
only be achieved when accounting for the HONO generated by the NaNO<sub>2</sub> exposed to humid air  
420 (~50 % RH). No other acidic or ionic contaminants were present in NaNO<sub>2</sub> reaction devices or the  
HCl PDs when scrubbed solutions were analyzed by IC-CD. Therefore, other NO<sub>y</sub> species that  
could have biased the NO<sub>x</sub> analyzer measurement high were judged to be absent and pure HONO  
was generated (i.e. only NO<sub>2</sub><sup>-</sup> was enhanced in calibration system flows scrubbed into 1 mM  
NaOH). Further investigation of the system HONO purity is presented in Section 3.7.3 which  
425 further supports this conclusion. The remainder of the HONO output from NaNO<sub>2</sub> devices  
quantitatively matched the HCl input to the reaction device in dry air after accounting for the water  
vapour production route. No HCl was observed to exit the devices, indicating unit acid  
displacement efficiency and reaching mass balance.

### 3.4.2 CIMS Measurements

430 Confirmation of these observations with the quadrupole CIMS provided higher time resolution  
observations of HONO and HCl simultaneously. The ions monitored were m/z 35 (Cl<sup>-</sup>) for HCl  
and 46 (NO<sub>2</sub><sup>-</sup>) for HONO (Figure 2). The instrumental sensitivity to these two analytes is similar  
under this ionisation scheme (VandenBoer et al., 2013). The HONO calibration source was  
stabilized for 2 h before the gas stream was introduced to the CIMS. Zero measurements were  
435 taken for 15 min before and after the measurements to correct for background drift in the m/z 46  
signal. Upon sampling the output of the HONO calibration source the signal at m/z 46 rapidly  
increased (Fig. 2). The signal of Cl<sup>-</sup> at m/z 35 was below the detection limit throughout this period,  
confirming again that the HCl from the PD was entirely consumed by the NaNO<sub>2</sub> reaction device  
throughout the measurement period, consistent with the experiments presented above where no  
440 HCl was measured by the CRDS. Overall, the results from these assessments indicate that the  
HONO calibration source is generating HONO with a one to one displacement efficiency by HCl,  
consistent with this observation from other HONO calibration sources using higher quantities of  
HCl in a salt bed (Febo et al., 1995; Roberts et al., 2010), and the remainder originating from the  
water vapour reaction.

445

### 3.5 Stability of HONO production

The time required to achieve stable HONO signals was tested by inserting HCl PD-6a and new  
NaNO<sub>2</sub> PFA reaction device into the calibration system, followed by flow start up. Stable HONO  
signals were observed within 7 h of powering on the HONO calibration system. This is 5 h longer  
450 than required to reach stable mixing ratios for a previously stabilized NaNO<sub>2</sub> device. Three trials  
using newly coated NaNO<sub>2</sub> reaction devices and PD-6a, once stabilized, generated an average

HONO output of  $2.28 \pm 0.58$  ppbv, which corresponds to an RSD of 24 % between runs and an RSE of 3% ( $n = 2367$ ; Figure 3). The noise observed in the stabilized HONO output in Figure 3 can be primarily attributed to the noise associated with the  $\text{NO}_x$  analyzer detector (18 of the 24 %; DL = 0.4 ppbv; 1-minute average). This conclusion is supported by the lower noise in  $\sim 2.5$  ppbv HONO mixing ratios observed by the CIMS (Fig. 2, RSD of 8.1%), ACES (RSD 8.2 %), and  $\text{NO}_y\text{O}_3$  (RSD 1.9 %). In these added observations with higher sensitivity instrumentation, the stability was equal to instrumental precision. This represents a major improvement over our previously reported calibration sources with potential for 30 % variability at a minimum (VandenBoer et al., 2013; Zhou et al., 2018).

However, when the HCl output from PDs is unstable, this can interfere with the stability of the HONO generated because it is dependent on acid displacement. A common characteristic of our custom-PDs monitored by real-time CRDS measurements are short-duration increases in output over min, up to 1 h, due to reduced emission of  $\text{H}_2\text{O}$  and increased emission of HCl, resulting in transient pulses from the device (Figure 4a). The anticorrelation between HCl and  $\text{H}_2\text{O}$  is expected for a constant mass emission to result from the contained aqueous solution. A corresponding rapid increase in HONO production results from such occurrences (Figure 4b).

Commercial PD manufacturers evaluate average mass emission rates by gravimetric weight loss over several weeks at 40 °C for certification, which could include such short-term events. The HONO output from a newly made custom-HCl PD (PD-6c) over four consecutive observation periods upon insertion of a new  $\text{NaNO}_2$  reaction device (Runs 1 – 4) at constant temperature (40 °C) show that the new custom-PD requires about 1 week of operation before its output is stable (Figure 4b-c). Therefore, careful preparation of PDs and  $\text{NaNO}_2$  reaction devices in advance of extensive use will yield a HONO calibration source with the fastest stabilization times possible for continuous operation over a period of months. Note again, that the HONO measurements for Figures 4b-c were performed several months before the HCl emission rate for PD-6c presented in Table 1 were obtained, resulting in high HONO mixing ratios produced in these experiments.

480

### 3.6 Reproducibility and robustness

The HONO calibration system was designed to not only be stable, but reproducible in its output of HONO for a given PD and any  $\text{NaNO}_2$  reaction device, resulting in robust portability. We tested the reproducibility, and therefore robustness, of the HONO calibration system by putting it through a series of experiments designed to simulate transport to, and use in, the field. Further assessment of its reproducibility by measuring the output with different  $\text{NaNO}_2$  reaction devices and HCl PDs were also made.

#### 3.6.1 Field transport simulations

Simulations of field transportation subjected the system to full disassembly and reassembly of the acid displacement and permeation oven setup. In addition, for some experiments the calibration

490

unit was transported on a lab cart over very rough flooring to simulate vibrations experienced for real use when transported using rolling carts, mobile labs, or aircraft. For the first eight simulations PD-6a and one NaNO<sub>2</sub> coated reaction device were used over several weeks (see Table S1 for further detail). Following reassembly after the field transport simulations, the HONO calibration source was restarted, the system was equilibrated for 2 hours, and then its output measured by the NO<sub>x</sub> analyzer (Figure 5). An Na<sub>2</sub>CO<sub>3</sub> coated annular denuder was incorporated into the middle of five of the eight trial experiments for an hour to determine whether any NO<sub>x</sub> was being generated between restarts and its associated variability (FS1-FS5; Table S1). No measurable NO<sub>x</sub> was detected in any of these experiments.

The average HONO mixing ratio within the eight field transport simulations (FS) ranged from 1.68 to 2.51 ppbv. The HONO output across all eight field simulations had an average of 2.07±0.48 ppbv (RSD = 24 %; RSE = 2 % (n = 218)). These measurements used a single NaNO<sub>2</sub> reaction device over 5 weeks of continuous operation, after which the depletion of NaNO<sub>2</sub> resulted in a decline of HONO mixing ratios. These HONO mixing ratios are similar to the average HONO output of 2.28±0.58 ppbv (RSD of 24 %; RSE of 3 % (n = 2367) from the previous measurements with PD-6a (Figure 3), which were not subject to field simulations but did use freshly coated NaNO<sub>2</sub> reaction devices. The generated HONO mixing ratios varied most between our early experiments (FS1-FS4; RSD ≥ 24 %), when first gaining experience in ensuring gas-tight connections throughout the calibration system, with improvement clearly emerging over time (FS4-FS8; RSD ≤ 10 %). The RSE values of field transport simulations had a lower RSE of 1 % compared to 3 % for the experiments that were stationary (Fig. 5), likely due to the reuse of the same NaNO<sub>2</sub> reaction device. This demonstrates that the HONO calibration source can robustly generate a reproducible mixing ratio output within 25 % of the mean during each system reconstruction if the same HCl PD is used. It is worth noting here again that most of the variance observed in HONO mixing ratio output within any of the presented trials derives from the precision of our NO<sub>x</sub> analyzer detector (Section 3.5).

### 3.6.2 Factors affecting reproducibility of HCl input

As shown in Table 1, PDs made with the same HCl concentration (6 M) and similar dimensions did not lead to the same HONO output, due to variability in the HCl emission rates. While it is possible for custom-made PDs to have similar HCl emissions and therefore HONO output (when using the same NaNO<sub>2</sub> device), it is difficult to achieve in practice. When making a new PD as per the methods described in Section S2, it can be difficult to replicate because the emission rate depends on the effectiveness of the plug seal. For this reason, one cannot simply make a HCl PD with plugs using the same concentration and material dimensions and necessarily expect the same output. We present an alternative Teflon welding method to overcome this limitation in Section S2 which has been successfully used for generation of VOC PDs. Regardless, the output of new HCl PDs should be quantified prior to use and not subject to extreme conditions to ensure the polymer permeability is retained.

The reproducibility of HONO output using a stable HCl PD is shown in Figure 5. The observed HONO output ranged from 1.68-2.51 ppbv (n=8, RSD = 24 %). We next tested the reproducibility for newly made HCl PDs. Two experiments used PD-6b, containing 6 M HCl (Figure S10). After a period of stabilization, the two experiments generated similar HONO mixing ratios (2.58±0.43 ppbv after 25 hrs, RSD = 16.5 %, RSE = 1.43 %, n = 792). The spikes in HONO output at 15 h and 21 h in the second experiment (green trace, Fig. S10) were likely due to pulses of HCl which we commonly observed with new PDs (e.g. Fig. 4a-b). This emphasizes our recommendation that new custom-HCl PDs should be used for an extended period prior to use for acid displacement to ensure the emission rate has stabilized.

We made another PD with 1.2 M HCl, as it emits less HCl in comparison to a PD made with 6 M HCl (Table 1), to determine the reproducibility in HONO output at lower mixing ratios. Across three experiments using a previously stabilized NaNO<sub>2</sub> device, an output of 0.69-1.12 ppbv (RSD = 53.7 %, RSE = 4.52 %, n = 143) was observed (Fig. S11). The high RSD is due to instrument noise as the HONO output approached the detection limit of the NO<sub>x</sub> analyzer (0.4 ppbv). Nonetheless, a stable output of HONO was achieved within two hours after starting the calibration system, similar to our previous results (Fig. 5). As long as a new custom-HCl PD has been allowed adequate time to stabilize under a gas flow at constant temperature (ideally 7 days), a stable HONO output can be easily replicated within two hours of starting the resulting HONO calibration system. We recommend quantifying the HCl emissions prior to use if the PD has been stored for a long period or been subjected to extreme conditions.

### 3.7 Adjusting and controlling HONO mixing ratios

Increasing the mixing ratio of HCl, and the type and quantity of NaNO<sub>2</sub> reaction devices connected in series were explored as methods to adjust the HONO mixing ratio exiting the calibration system.

#### 3.7.1 Temperature control

The HONO calibration system was designed to be tunable by adjusting the oven temperature. HCl emissions increased with increasing temperatures (30 °C – 60 °C, Fig. S6), The HONO mixing ratios increased exponentially with increasing oven temperatures (Table 3 and Fig. S12). Very low levels of HCl exited the NaNO<sub>2</sub> device (≤ 3% of HCl input), which demonstrated that there was continued near-unity acid displacement efficiency. With increasing temperature of the NaNO<sub>2</sub> reaction device in the presence of water vapour, a similar increase in HONO mixing ratio was observed, roughly doubling for every increase of 10 °C. Thus, the HONO mixing ratio output can be adjusted by changing the temperature of the Al-block with either water vapour alone or in combination with an HCl PD. Part of the observed variability in HONO emissions at 50 °C was contributed by the increasingly unstable emissions of HCl at this temperature (e.g. see Fig. S6). The use of multiple HCl permeation tubes in a single oven, in series, or in parallel are additional options to control the HONO mixing ratio generated in the calibration system.

### 3.7.2 HONO output with different types of NaNO<sub>2</sub>-coated devices

570 The produced HONO mixing ratios were tested using different materials coated with NaNO<sub>2</sub> via  
the same methodology as the PFA devices (Section 2.1) to see if there was an improvement in  
output stability or increased emissions of HONO. The materials used were all cylindrical tubing  
with ½” (1.27 cm) inner diameters and were of similar lengths and surface area. The different  
materials that were tested showed similar HONO outputs (within variability), except for quartz  
575 (Table 4). The quartz tubing gave a notably lower HONO output compared to other materials. This  
may have been due to a poor coating efficiency on the surface, as observed visually when making  
this device. This is an unexpected outcome given that quartz is more hydrophilic than PFA. That  
we observed similar HONO outputs for the other materials could be due to the devices having the  
same internal surface area coated with NaNO<sub>2</sub>, implying that HONO output is proportional to  
surface-available NaNO<sub>2</sub>. The inside of a PFA device was etched manually every few mm in  
580 concentric circles in an attempt to increase the surface availability of NaNO<sub>2</sub>, but no change HONO  
output was observed compared to the unetched device.

Two additional methods were tested to increase the available surface area in the NaNO<sub>2</sub> device:  
increasing the number of coated PFA reaction devices in series and using an annular denuder. The  
HONO output with two PFA devices connected in series increased when using either 2.0 ppbv  
585 (PD-6b) or 5.0 ppbv of HCl (PD-6c) at 40 °C and 50 % RH. We did not observe HCl breakthrough  
at the exit of the first PFA device, indicating that the increased HONO mixing ratio is the result of  
the water vapour reaction. We observed variability in the amount of HONO produced between the  
four PFA devices, ranging from 0.8 to 1.3 ppbv per device.

More HONO can be generated using the same PDs in conjunction with an annular denuder, which  
590 has a larger internal surface area of 3063 cm<sup>2</sup> compared to 388 cm<sup>2</sup> for the PFA device. HONO  
emissions using PD-6c and an annular denuder produced a factor of four higher mixing ratio 24.5  
±1.0 ppbv compared to 6.2 ±0.5 ppbv with a single PFA device, but it required 45 hours to stabilize.  
Again, the increase is due to promotion of the water vapour reaction. The major drawback of using  
an annular denuder is that the output drifted to lower mixing ratios continuously at a rate of a few  
595 ppbv per hour, which was not a feature of the PFA devices (Figure 6). The HONO output over  
any 4 hour period was reasonably stable (within 0.5 ppbv) following the first 24 hours of  
stabilization time, which suggests that a NaNO<sub>2</sub> coated annular denuder could be viable for short  
duration HONO calibrations if a secondary quantitative method is available to confirm its output  
(e.g. a NO<sub>x</sub> analyzer with a quantified HONO conversion efficiency). Overall, using a NaNO<sub>2</sub>  
600 coated annular denuder can provide higher HONO outputs than using PFA devices but requires at  
least daily independent verification.

### 3.7.3 Purity of the HONO output

Previous work has demonstrated that there can be a notable NO<sub>x</sub> impurity when generating HONO  
via the acid displacement method (Febo et al., 1995). To test the purity of the calibration source,  
605 the HONO output was analysed by additional reactive nitrogen, NO<sub>x</sub>, and NO<sub>y</sub> instrumentation.



For these experiments, we used a 6 M HCl PD and two PFA devices in series in a 40 °C calibration system, which was determined to have an output of 770 pptv of HONO. First, the output was analysed by an I<sup>-</sup> ToF CIMS and found no evidence for any detectable amounts of other nitrogen containing species (e.g. ClNO<sub>2</sub>, ClNO, HNO<sub>3</sub>; Figure S13) except for HONO (Neuman et al., 2016; Veres et al., 2020). The I<sup>-</sup> TOF CIMS is not sensitive to NO or NO<sub>2</sub>, so further measurements were made with our Mo-catalyst NO<sub>x</sub> analyzer, a cavity-enhanced absorption spectrometer (Min et al., 2016), and a gold-catalyst NO<sub>y</sub> instrument (Fahey et al., 1985; Fontijn et al., 1970; Ridley and Grahek, 1990; Ridley and Howlett, 1974; Ryerson et al., 1999), which determined that NO<sub>2</sub> impurities were at or below 10 % of the generated HONO based on the detection precisions of the latter two instruments. Finally, we quantified NO impurities using a single-photon LIF instrument, which is sensitive to sub-pptv levels of NO (Rollins et al., 2020). We observed NO at 5.5 % of the measured HONO signal (42 versus 770 pptv). Examination of our modified NO<sub>x</sub> analyzer experiments using the same calibration system configuration revealed 6 % NO on average compared to the observed HONO (ca. 6-9 ppbv), consistent with the LIF measurements. In contrast, when using a NaNO<sub>2</sub>-coated annular denuder with the same HCl PD, our modified NO<sub>x</sub> analyzer observed NO/HONO to decrease to 2%.

Recent work, using an analogous HONO calibration system, has found high production of NO, NO<sub>2</sub> and ClNO (> 10 %) when HCl input to loose NaNO<sub>2</sub> was > 4 ppmv (Gingerysty and Osthoff, 2020). We observed similarly high output of NO when the HCl input was increased to 2.4 ppmv through the NaNO<sub>2</sub>-coated devices. Under these conditions, the impurity may be due to self-reactions of HONO at high mixing ratios, as seen in other packed or stirred NaNO<sub>2</sub> salt beds (Febo et al., 1995). NO impurities at HONO mixing ratios below 100 ppbv in the salt bed may result from other heterogeneous processes generating NO in the lower HONO production regime. It may be that such small absolute quantities of NO have been produced in all prior calibration sources, but as the mixing ratio of HONO produced has been reduced in our calibration system, that this impurity increases in a relative sense. The purity of the calibration source when generating < 100 ppbv in the salt bed is ≥ 90 % HONO, with the remainder accounted for as NO and/or NO<sub>2</sub>.

### 3.8 Context and application

The RSE of our stable HONO output is < 2.5% and less than previous HCl acid displacement calibration source adaptations (VandenBoer et al., 2013; Zhou et al., 2018). Potential reasons for the improved stability in HONO output are the stable production of HCl from custom-PDs and that the calibration system presented in the current work eliminated the need for solid NaNO<sub>2</sub> powder, which is prone to disturbance of equilibrated emissions through vibrations that can result in changes up to a factor of two in mixing ratio output (VandenBoer et al., 2013; Zhou et al., 2018). The RSD at the low HONO mixing ratios in this work are larger than reported by Febo et al. (1995), who generated much larger mixing ratios, but did not specify the measurement details of their NO<sub>x</sub> analyzer to facilitate true comparison. The greatest accuracy possible for this calibration source requires quantitation of the HONO output by a separate analytical method (e.g. IC-CD) and

645 should not rely on the assumption that the HONO generated is equivalent to the HCl delivered into  
the reaction device due to the additional production mechanism driven by water vapour. While the  
output of this system is demonstrated to be highly reproducible with a given HCl PD, we  
recommend regular calibration.

## 650 **4 Conclusions**

We present a cost-effective, portable, stable, tunable, and robust gas-phase HONO calibration  
source. We utilised both a water vapour only, as well as its combination with the acid displacement  
reaction of HCl, with sodium nitrite ( $\text{NaNO}_2$ ) coated on the inner wall of a short length of PFA  
tubing within a machined Al-block permeation oven to produce a stable and continuous supply of  
655 high purity gaseous HONO. We demonstrated for the first time that HONO was produced by  
humid air in the  $\text{NaNO}_2$  reaction device, such that the HONO output was consistently higher than  
the HCl input. If a HONO calibration source in the pptv range was desired, it could be achieved  
easily by using only humid air flowing through an  $\text{NaNO}_2$  coated reaction device. The output of  
this HONO calibration source spans the range of environmentally relevant mixing ratios - from  
660 pptv levels to tens of ppbv. This will allow instruments to be calibrated and/or intercompared using  
their standard atmospheric sampling parameters, without the need for excessive - or impossible -  
dilution; nor additional pumps, valves, and mass flow controllers.

We demonstrated that our HONO calibration system mixing ratio was tunable by adjusting the  
temperature of the permeation oven to control the water vapour reaction, as well as HCl emission  
rates from PDs. The HONO calibration source was designed to facilitate multiple calibrant  
665 concentrations, as the four holes in the aluminium heating block (Fig. S3) allows for the operation  
of parallel HONO sources if desired. The most stable HONO output was achieved using  $\text{NaNO}_2$   
coated PFA devices at 40 °C, with HONO mixing ratios of  $2.28 \pm 0.58$  ppbv (RSD of 24 % and  
RSE of 3%,  $n = 8$ ) that were reliably reproduced following complete assembly of the system. From  
670 our wide range of instrumental observations, the output of the source appears to be constant within  
 $\pm 10$  % or better. The purity of HONO source was determined to be  $>90\%$ , and while lower than  
previous work (99.5%, Febo *et al.* (1995)) this may be a consequence of previously unseen side  
reactions of increasing importance at the low HONO mixing ratios generated. We consider this an  
acceptable trade-off for a robust field deployable HONO source unit. The resulting system can be  
675 disassembled, transported, and reassembled to produce the same HONO mixing ratios  
reproducibly, without the need for regular maintenance - where the same PD is retained between  
rebuids. Custom-made HCl PDs are prone to variability in emission rates, both between similarly  
made PDs and over time, and therefore require regular characterization, but can provide a stable  
output over the order of weeks. While higher HONO outputs were possible to generate using an  
680  $\text{NaNO}_2$  coated annular denuder for any given HCl PD, the outputs were unstable over time.

This HONO calibration instrument provides a universal solution to gas-phase HONO calibrations  
suitable for the full range of atmospheric instrumentation used for outdoor or indoor field

685 measurements or laboratory experiments. This calibration unit could be used to intercompare the responses/measurements between HONO instruments to investigate and validate accuracy and precision of their ambient measurements in addition to identifying and isolating potential interferences (Crilley et al., 2019). We anticipate it will also find utility in the generation of isotopically-labelled HONO for the emerging exploration of stable-isotopic composition of HONO and its relation to the wide variety of suspected atmospheric HONO sources (Chai et al., 2019).

### **Author Contributions**

690 TV, CY, and RW conceptualized the calibration source. TV and CY supervised the experiments, acquired the funding, and provided the resources to support this work. TV designed the experiments, guided the investigations, and managed the project. ML constructed the custom PDs under the guidance of TF and LS. ML and LS built the custom permeation oven and analyzed IC-CD samples. LC and ML performed the mass balance, reaction device, and purity experiments.  
695 LC and ML established and validated the methodologies. IB, AN, DR, PV, RW and CW provided instrumental resources, and performed measurements included in the stability and purity experiments. LS created the schematics and wrote the detailed description of the custom permeation oven. ML constructed the reaction devices, performed part - or the entirety - of the experiments, and prepared the manuscript with contributions from all authors. All authors  
700 participated in data analysis, and the review and editing of the manuscript.

*The authors declare that they have no conflict of interest.*

### **Acknowledgments**

705 The Authors thank E Gaona-Colman for help in collecting the CIMS data, as well as J Liggio and J Wentzell for enabling the use of and training on the quadrupole CIMS. ML acknowledges research support from an NSERC Undergraduate Student Research Award, and travel support through a York University Fieldwork Cost Fund award, respectively. LS acknowledges research support from the Harold I Schiff graduate award in Atmospheric Chemistry. LC and TV acknowledge travel support from the York University Faculty of Science Junior Faculty Fund. CY  
710 acknowledges support for this project through an NSERC Discovery Grant. TV and CY acknowledge funding for the instrumentation developed and used in this work provided by the Alfred P. Sloan Foundation Chemistry of Indoor Environments program (G-2018-11051).

### **Data Availability**

715 Datasets are presented in figures and summarized in tables throughout the main manuscript and supporting information. Raw data from these resources are available from the corresponding author upon request.

## References

- 720 Braman, R. S. and de la Cantera, M. A.: Sublimation sources for nitrous acid and other nitrogen compounds in air, *Anal. Chem.*, 58(7), 1533–1537, doi:10.1021/ac00298a059, 1986.
- 725 Chai, J., Miller, D. J., Scheuer, E., Dibb, J., Selimovic, V., Yokelson, R., Zarzana, K. J., Brown, S. S., Koss, A. R., Warneke, C. and Hastings, M.: Isotopic characterization of nitrogen oxides ( $\text{NO}_x$ ), nitrous acid (HONO), and nitrate ( $\text{pNO}_3^-$ ) from laboratory biomass burning during FIREX, *Atmos. Meas. Tech.*, 12, 6303–6317, doi:10.5194/amt-2019-229, 2019.
- 730 Cheng, P., Cheng, Y., Lu, K., Su, H., Yang, Q., Zou, Y., Zhao, Y., Dong, H., Zeng, L. and Zhang, Y.: An online monitoring system for atmospheric nitrous acid (HONO) based on stripping coil and ion chromatography, *J. Environ. Sci. (China)*, 25(5), 895–907, doi:10.1016/S1001-0742(12)60251-4, 2013.
- 735 Collins, D. B., Hems, R. F., Zhou, S., Wang, C., Grignon, E., Alavy, M., Siegel, J. A. and Abbatt, J. P. D.: Evidence for gas-surface equilibrium control of indoor nitrous acid, *Environ. Sci. Technol.*, 52(21), 12419–12427, doi:10.1021/acs.est.8b04512, 2018.
- 740 Crilley, L. R., Kramer, L., Pope, F. D., Whalley, L. K., Cryer, D. R., Heard, D. E., Lee, J. D., Reed, C. and Bloss, W. J.: On the interpretation of in situ HONO observations via photochemical steady state, *Faraday Discuss.*, 189, 191–212, doi:10.1039/c5fd00224a, 2016.
- 745 Crilley, L. R., Kramer, L. J., Ouyang, B., Duan, J., Zhang, W., Tong, S., Ge, M., Tang, K., Qin, M., Xie, P., Shaw, M. D., Lewis, A. C., Mehra, A., Bannan, T. J., Worrall, S. D., Priestley, M., Bacak, A., Coe, H., Allan, J., Percival, C. J., Popoola, O. A. M., Jones, R. L. and Bloss, W. J.: Intercomparison of nitrous acid (HONO) measurement techniques in a megacity (Beijing), *Atmos. Meas. Tech.*, 12, 6449–6463, doi:10.5194/amt-12-6449-2019, 2019.
- 750 Dawe, K. E. R., Furlani, T. C., Kowal, S. F., Kahan, T. F., VandenBoer, T. C. and Young, C. J.: Formation and emission of hydrogen chloride in indoor air, *Indoor Air*, 29(1), doi:10.1111/ina.12509, 2019.
- 755 Elshorbany, Y. F., Kurtenbach, R., Wiesen, P., Lissi, E., Rubio, M., Villena, G., Gramsch, E., Rickard, A. R., Pilling, M. J. and Kleffmann, J.: Oxidation capacity of the city air of Santiago, Chile, *Atmos. Chem. Phys.*, 9(6), 2257–2273, doi:10.5194/acp-9-2257-2009, 2009.
- Fahey, D. W., Eubank, C. S., Hübler, G. and Fehsenfeld, F. C.: Evaluation of a catalytic reduction technique for the measurement of total reactive odd-nitrogen  $\text{NO}_y$  in the atmosphere, *J. Atmos. Chem.*, 3(4), 435–468, doi:10.1007/BF00053871, 1985.
- 760 Febo, A., Perrino, C., Gherardi, M. and Sparapani, R.: Evaluation of a high-purity and high-stability continuous generation system for nitrous acid, *Environ. Sci. Technol.*, 29(9), 2390–2395, doi:10.1021/es00009a035, 1995.
- Febo, A., Perrino, C. and Allegrini, I.: Measurement of nitrous acid in Milan, Italy, by DOAS and

- 765 diffusion denuders, *Atmos. Environ.*, 30(21), 3599–3609, doi:10.1016/1352-2310(96)00069-6, 1996.
- Fontijn, A., Sabadell, A. J. and Ronco, R. J.: Homogeneous chemiluminescent measurement of nitric oxide with ozone: Implications for continuous selective monitoring of gaseous air pollutants, *Anal. Chem.*, 42(6), 575–579, doi:10.1021/ac60288a034, 1970.
- 770
- Fried, A., Henry, B. and Sewell, S.: Potential calibration errors in carbonyl sulfide permeation devices: Implications for atmospheric studies, *J. Geophys. Res. Atmos.*, 103(D15), 18895–18906, doi:10.1029/98JD00620, 1998.
- 775
- Gall, E. T., Griffin, R. J., Steiner, A. L., Dibb, J., Scheuer, E., Gong, L., Rutter, A. P., Cevik, B. K., Kim, S., Lefer, B. and Flynn, J.: Evaluation of nitrous acid sources and sinks in urban outflow, *Atmos. Environ.*, 127, 272–282, doi:10.1016/j.atmosenv.2015.12.044, 2016.
- 780
- Gingerysty, N. J. and Osthoff, H. D.: A compact , high-purity source of HONO validated by Fourier transform infrared and thermal dissociation cavity ring-down spectroscopy, *Atmos. Meas. Tech. Discuss.*, 1–20, doi:10.5194/amt-2020-92, 2020.
- 785
- Gligorovski, S.: Nitrous acid (HONO): An emerging indoor pollutant, *J. Photochem. Photobiol. A Chem.*, 314, 1–5, doi:10.1016/j.jphotochem.2015.06.008, 2016.
- Gómez Alvarez, E., Wortham, H., Strekowski, R., Zetzsch, C. and Gligorovski, S.: Atmospheric photosensitized heterogeneous and multiphase reactions: From outdoors to indoors, *Environ. Sci. Technol.*, 46(4), 1955–1963, doi:10.1021/es2019675, 2012.
- 790
- Harris, G. W., Carter, W. P. L., Winer, A. M., Pitts, J. N., Platt, U. and Perner, D.: Observations of Nitrous Acid in the Los Angeles Atmosphere and Implications for Predictions of Ozone—Precursor Relationships, *Environ. Sci. Technol.*, 16(7), 414–419, doi:10.1021/es00101a009, 1982.
- 795
- Heland, J., Kleffmann, J., Kurtenbach, R. and Wiesen, P.: A new instrument to measure gaseous nitrous acid (HONO) in the atmosphere, *Environ. Sci. Technol.*, 35(15), 3207–3212, doi:10.1021/es000303t, 2001.
- 800
- Honrath, R. E., Lu, Y., Peterson, M. C., Dibb, J. E., Arsenault, M. A., Cullen, N. J. and Steffen, K.: Vertical fluxes of NO<sub>x</sub>, HONO, and HNO<sub>3</sub> above the snowpack at Summit, Greenland, *Atmos. Environ.*, 36(15–16), 2629–2640, doi:10.1016/S1352-2310(02)00132-2, 2002.
- 805
- Kasibhatla, P., Sherwen, T., Evans, M. J., Carpenter, L. J., Reed, C., Alexander, B., Chen, Q., Sulprizio, M. P., Lee, J. D., Read, K. A., Bloss, W., Crilley, L. R., Keene, W. C., Pszenny, A. A. P. and Hodzic, A.: Global impact of nitrate photolysis in sea-salt aerosol on NO<sub>x</sub>, OH, and O<sub>3</sub> in the marine boundary layer, *Atmos. Chem. Phys.*, 18(15), 11185–11203, doi:10.5194/acp-18-11185-2018, 2018.
- 810
- Kim, S., VandenBoer, T. C., Young, C. J., Riedel, T. P., Thornton, J. A., Swarthout, B., Sive, B., Lerner, B., Gilman, J. B., Warneke, C., Roberts, J. M., Guenther, A., Wagner, N. L., Dubé, W. P.,

- Williams, E. and Brown, S. S.: The primary and recycling source of OH during the NACHTT-2011 campaign: HONO as an important OH primary source in the wintertime, *J. Geophys. Res. Atmos.*, 119, 6886–6896, doi:10.1002/2013JD021186, 2014.
- 815 Kleffmann, J.: Daytime sources of nitrous acid (HONO) in the atmospheric boundary layer, *ChemPhysChem*, 8(8), 1137–1144, doi:10.1002/cphc.200700016, 2007.
- Kleffmann, J. and Wiesen, P.: Technical Note: Quantification of interferences of wet chemical HONO LOPAP measurements under simulated polar conditions, *Atmos. Chem. Phys.*, 8(22), 6813–6822, doi:10.5194/acp-8-6813-2008, 2008.
- 820
- Kleffmann, J., Benter, T. and Wiesen, P.: Heterogeneous reaction of nitric acid with nitric oxide on glass surfaces under simulated atmospheric conditions, *J. Phys. Chem. A*, 108(27), 5793–5799, doi:10.1021/jp040184u, 2004.
- 825
- Kleffmann, J., Lörzer, J. C., Wiesen, P., Kern, C., Trick, S., Volkamer, R., Rodenas, M. and Wirtz, K.: Intercomparison of the DOAS and LOPAP techniques for the detection of nitrous acid (HONO), *Atmos. Environ.*, 40(20), 3640–3652, doi:10.1016/j.atmosenv.2006.03.027, 2006.
- 830
- Lee, B. H., Wood, E. C., Herndon, S. C., Lefer, B. L., Luke, W. T., Brune, W. H., Nelson, D. D., Zahniser, M. S. and Munger, J. W.: Urban measurements of atmospheric nitrous acid: A caveat on the interpretation of the HONO photostationary state, *J. Geophys. Res. Atmos.*, 118(21), 12274–12281, doi:10.1002/2013JD020341, 2013.
- 835
- Lee, J. D., Whalley, L. K., Heard, D. E., Stone, D., Dunmore, R. E., Hamilton, J. F., Young, D. E., Allan, J. D., Laufs, S. and Kleffmann, J.: Detailed budget analysis of HONO in central London reveals a missing daytime source, *Atmos. Chem. Phys.*, 16(5), 2747–2764, doi:10.5194/acp-16-2747-2016, 2016.
- 840
- Liu, J., Li, S., Zeng, J., Mekic, M., Yu, Z., Zhou, W., Loisel, G., Gandolfo, A., Song, W., Wang, X., Zhou, Z., Herrmann, H., Li, X. and Gligorovski, S.: Assessing indoor gas phase oxidation capacity through real-time measurements of HONO and NO<sub>x</sub> in Guangzhou, China, *Environ. Sci. Process. Impacts*, 21(8), 1393–1402, doi:10.1039/c9em00194h, 2019.
- 845
- MacInnis, J. J., VandenBoer, T. C. and Young, C. J.: Development of a gas phase source for perfluoroalkyl acids to examine atmospheric sampling methods, *Analyst*, 141(12), doi:10.1039/c6an00313c, 2016.
- 850
- McGrath, D. T., Ryan, M. D., Macinnis, J. J., Vandenboer, T. C., Young, C. J. and Katz, M. J.: Selective decontamination of the reactive air pollutant nitrous acid via node-linker cooperativity in a metal-organic framework, *Chem. Sci.*, 10(21), 5576–5581, doi:10.1039/c9sc01357a, 2019.
- 855
- Min, K. E., Washenfelder, R. A., Dubé, W. P., Langford, A. O., Edwards, P. M., Zarzana, K. J., Stutz, J., Lu, K., Rohrer, F., Zhang, Y. and Brown, S. S.: A broadband cavity enhanced absorption spectrometer for aircraft measurements of glyoxal, methylglyoxal, nitrous acid, nitrogen dioxide, and water vapor, *Atmos. Meas. Tech.*, 9(2), 423–440, doi:10.5194/amt-9-423-2016, 2016.

- Mitchell, G. D.: A review of permeation tubes and permeators, *Sep. Purif. Methods*, 29(1), 119–128, doi:10.1081/SPM-100100005, 2000.
- 860 Mushinski, R. M., Phillips, R. P., Payne, Z. C., Abney, R. B., Jo, I., Fei, S., Pusede, S. E., White, J. R., Rusch, D. B. and Raff, J. D.: Microbial mechanisms and ecosystem flux estimation for aerobic NO<sub>y</sub> emissions from deciduous forest soils, *Proc. Natl. Acad. Sci. U. S. A.*, 116(6), 2138–2145, doi:10.1073/pnas.1814632116, 2019.
- 865 Neuman, J. A., Ryerson, T. B., Huey, L. G., Jakoubek, R., Nowak, J. B., Simons, C. and Fehsenfeld, F. C.: Calibration and evaluation of nitric acid and ammonia permeation tubes by UV optical absorption, *Environ. Sci. Technol.*, 37(13), 2975–2981, doi:10.1021/es0264221, 2003.
- 870 Neuman, J. A., Trainer, M., Brown, S. S., Min, K. E., Nowak, J. B., Parrish, D. D., Peischl, J., Pollack, I. B., Roberts, J. M., Ryerson, T. B. and Veres, P. R.: HONO emission and production determined from airborne measurements over the Southeast U.S., *J. Geophys. Res. Atmos.*, 121(15), 9237–9250, doi:10.1002/2016JD025197, 2016.
- 875 O’Keeffe, A. E. and Ortman, G. C.: Primary standards for trace gas analysis, *Anal. Chem.*, 38(6), 760–763, doi:10.1021/ac60238a022, 1966.
- 880 Oswald, R., Behrendt, T., Ermel, M., Wu, D., Su, H., Cheng, Y., Breuninger, C., Moravek, A., Mougín, E., Delon, C., Loubet, B., Pommerening-Röser, A., Sörgel, M., Pöschl, U., Hoffmann, T., Andreae, M. O., Meixner, F. X. and Trebs, I.: HONO emissions from soil bacteria as a major source of atmospheric reactive nitrogen, *Science* (80-. ), 341(6151), 1233–1235, doi:10.1126/science.1242266, 2013.
- 885 Pinto, J. P., Dibb, J., Lee, B. H., Rappenglück, B., Wood, E. C., Levy, M., Zhang, R. Y., Lefer, B., Ren, X. R., Stutz, J., Tsai, C., Ackermann, L., Golovko, J., Herndon, S. C., Oakes, M., Meng, Q. Y., Munger, J. W., Zahniser, M. and Zheng, J.: Intercomparison of field measurements of nitrous acid (HONO) during the SHARP campaign, *J. Geophys. Res. Atmos.*, 119(9), 5583–5601, doi:10.1002/2013JD020287, 2014.
- 890 Place, B. K., Young, C. J., Ziegler, S. E., Edwards, K. A., Salehpoor, L. and VandenBoer, T. C.: Passive sampling capabilities for ultra-trace quantitation of atmospheric nitric acid (HNO<sub>3</sub>) in remote environments, *Atmos. Environ.*, 191, 360–369, doi:10.1016/j.atmosenv.2018.08.030, 2018.
- 895 Pusede, S. E., VandenBoer, T. C., Murphy, J. G., Markovic, M. Z., Young, C. J., Veres, P. R., Roberts, J. M., Washenfelder, R. A., Brown, S. S., Ren, X., Tsai, C., Stutz, J., Brune, W. H., Browne, E. C., Wooldridge, P. J., Graham, A. R., Weber, R., Goldstein, A. H., Dusanter, S., Griffith, S. M., Stevens, P. S., Lefer, B. L. and Cohen, R. C.: An atmospheric constraint on the NO<sub>2</sub> dependence of daytime near-surface nitrous acid (HONO), *Environ. Sci. Technol.*, 49(21), 12774–12781, doi:10.1021/acs.est.5b02511, 2015.
- 900 Reed, C., Evans, M. J., Crilley, L. R., Bloss, W. J., Sherwen, T., Read, K. A., Lee, J. D. and

- 905 Carpenter, L. J.: Evidence for renoxification in the tropical marine boundary layer, *Atmos. Chem. Phys.*, 17(6), 4081–4092, doi:10.5194/acp-17-4081-2017, 2017.
- Ren, X., Gao, H., Zhou, X., Crounse, J. D., Wennberg, P. O., Browne, E. C., LaFranchi, B. W., Cohen, R. C., McKay, M., Goldstein, A. H. and Mao, J.: Measurement of atmospheric nitrous acid at Bodgett forest during BEARPEX2007, *Atmos. Chem. Phys.*, 10(13), 6283–6294, doi:10.5194/acp-10-6283-2010, 2010.
- 910 Ridley, B. A. and Grahek, F. E.: A small, low flow, high sensitivity reaction vessel for NO chemiluminescence detectors, *J. Am. Meteorol. Soc.*, 7, 307–311, 1990.
- Ridley, B. A. and Howlett, L. C.: An instrument for nitric oxide measurements in the stratosphere, 915 *Rev. Sci. Instrum.*, 45(6), 742–746, 1974.
- Roberts, J. M., Veres, P., Warneke, C., Neuman, J. A., Washenfelder, R. A., Brown, S. S., Baasandorj, M., Burkholder, J. B., Burling, I. R., Johnson, T. J., Yokelson, R. J. and De Gouw, J.: 920 Measurement of HONO, HNCO, and other inorganic acids by negative-ion proton-transfer chemical-ionization mass spectrometry (NI-PT-CIMS): Application to biomass burning emissions, *Atmos. Meas. Tech.*, 3(4), 981–990, doi:10.5194/amt-3-981-2010, 2010.
- Rollins, A. W., Rickly, P. S., Gao, R.-S., Ryerson, T. B., Brown, S. S., Peischl, J. and Bourgeois, 925 I.: Single-photon laser-induced fluorescence detection of nitric oxide at sub-parts per trillion mixing ratios, *Atmos. Meas. Tech.*, 13, 2425–2439, doi:10.5194/amt-13-2425-2020, 2020.
- Rubio, M. A., Lissi, E., Villena, G., Elshorbany, Y. F., Kleffmann, J., Kurtenbach, R. and Wiesen, P.: Simultaneous measurements of formaldehyde and nitrous acid in dew and gas phase in the 930 atmosphere of Santiago, Chile, *Atmos. Environ.*, 43(38), 6106–6109, doi:10.1016/j.atmosenv.2009.09.017, 2009.
- Ryerson, T. B., Huey, L. G., Knapp, K., Neuman, J. A., Parrish, D. D., Sueper, D. T. and Fehsenfeld, F. C.: Design and initial characterization of an inlet for gas-phase NO<sub>y</sub> measurements 935 from aircraft, *J. Geophys. Res.*, 104(D5), 5483–5492, 1999.
- Sörgel, M., Trebs, I., Serafimovich, A., Moravek, A., Held, A. and Zetzsch, C.: Simultaneous HONO measurements in and above a forest canopy: Influence of turbulent exchange on mixing 940 ratio differences, *Atmos. Chem. Phys.*, 11(2), 841–855, doi:10.5194/acp-11-841-2011, 2011.
- Sörgel, M., Trebs, I., Wu, D. and Held, A.: A comparison of measured HONO uptake and release with calculated source strengths in a heterogeneous forest environment, *Atmos. Chem. Phys.*, 15(16), 9237–9251, doi:10.5194/acp-15-9237-2015, 2015.
- 945 Spataro, F. and Ianniello, A.: Sources of atmospheric nitrous acid: State of the science, current research needs, and future prospects, *J. Air Waste Manag. Assoc.*, 64(11), 1232–1250, doi:10.1080/10962247.2014.952846, 2014.
- Stutz, J., Kim, E. S., Platt, U., Bruno, P., Perrino, C. and Febo, A.: UV-visible absorption cross



- 950 sections of nitrous acid, *J. Geophys. Res. Atmos.*, 105(D11), 14585–14592, doi:10.1029/2000JD900003, 2000.
- Stutz, J., Oh, H. J., Whitlow, S. I., Anderson, C., Dibb, J. E., Flynn, J. H., Rappenglück, B. and Lefer, B.: Simultaneous DOAS and mist-chamber IC measurements of HONO in Houston, TX, *Atmos. Environ.*, 44(33), 4090–4098, doi:10.1016/j.atmosenv.2009.02.003, 2010.
- 955 Susaya, J., Kim, K. H., Cho, J. and Parker, D.: The controlling effect of temperature in the application of permeation tube devices in standard gas generation, *J. Chromatogr. A*, 1225, 8–16, doi:10.1016/j.chroma.2011.12.066, 2012.
- 960 Taira, M. and Kanda, Y.: Continuous generation system for low-concentration gaseous nitrous acid, *Anal. Chem.*, 62(6), 630–633, doi:10.1021/ac00205a018, 1990.
- Tong, S., Hou, S., Zhang, Y., Chu, B., Liu, Y., He, H., Zhao, P. and Ge, M.: Exploring the nitrous acid (HONO) formation mechanism in winter Beijing: Direct emissions and heterogeneous production in urban and suburban areas, *Faraday Discuss.*, 189, 213–230, doi:10.1039/c5fd00163c, 2016.
- 965 Tsai, C., Spolaor, M., Fedele Colosimo, S., Pikelnaya, O., Cheung, R., Williams, E., Gilman, J. B., Lerner, B. M., Zamora, R. J., Warneke, C., Roberts, J. M., Ahmadov, R., De Gouw, J., Bates, T., Quinn, P. K. and Stutz, J.: Nitrous acid formation in a snow-free wintertime polluted rural area, *Atmos. Chem. Phys.*, 18(3), 1977–1996, doi:10.5194/acp-18-1977-2018, 2018.
- VandenBoer, T. C., Brown, S. S., Murphy, J. G., Keene, W. C., Young, C. J., Pszenny, A. A. P., Kim, S., Warneke, C., De Gouw, J. A., Maben, J. R., Wagner, N. L., Riedel, T. P., Thornton, J. A., Wolfe, D. E., Dubé, W. P., Öztürk, F., Brock, C. A., Grossberg, N., Lefer, B., Lerner, B., Middlebrook, A. M. and Roberts, J. M.: Understanding the role of the ground surface in HONO vertical structure: High resolution vertical profiles during NACHTT-11, *J. Geophys. Res. Atmos.*, 118(17), 10155–10171, doi:10.1002/jgrd.50721, 2013.
- 975 VandenBoer, T. C., Markovic, M. Z., Sanders, J. E., Ren, X., Pusede, S. E., Browne, E. C., Cohen, R. C., Zhang, L., Thomas, J., Brune, W. H. and Murphy, J. G.: Evidence for a nitrous acid (HONO) reservoir at the ground surface in Bakersfield, CA, during CalNex 2010, *J. Geophys. Res. Atmos.*, 119, 9093–9106, doi:10.1002/2013JD020971, 2014.
- 980 VandenBoer, T. C., Young, C. J., Talukdar, R. K., Markovic, M. Z., Brown, S. S., Roberts, J. M. and Murphy, J. G.: Nocturnal loss and daytime source of nitrous acid through reactive uptake and displacement, *Nat. Geosci.*, 8(1), 55–60, doi:10.1038/ngeo2298, 2015.
- 985 Večeřa, Z. and Dasgupta, P. K.: Measurement of ambient nitrous acid and a reliable calibration source for gaseous nitrous acid, *Environ. Sci. Technol.*, 25(2), 255–260, doi:10.1021/es00014a006, 1991.
- 990 Veres, P., Gilman, J. B., Roberts, J. M., Kuster, W. C., Warneke, C., Burling, I. R. and De Gouw, J.: Development and validation of a portable gas phase standard generation and calibration system

- 995 for volatile organic compounds, *Atmos. Meas. Tech.*, 3(3), 683–691, doi:10.5194/amt-3-683-2010, 2010a.
- Veres, P., Roberts, J. M., Burling, I. R., Warneke, C., De Gouw, J. and Yokelson, R. J.: Measurements of gas-phase inorganic and organic acids from biomass fires by negative-ion  
1000 proton-transfer chemical-ionization mass spectrometry, *J. Geophys. Res. Atmos.*, 115(23), D23302, doi:10.1029/2010JD014033, 2010b.
- Veres, P. R., Andrew Neuman, J., Bertram, T. H., Assaf, E., Wolfe, G. M., Williamson, C. J.,  
1005 Weinzierl, B., Tilmes, S., Thompson, C. R., Thames, A. B., Schroder, J. C., Saiz-Lopez, A., Rollins, A. W., Roberts, J. M., Price, D., Peischl, J., Nault, B. A., Møller, K. H., Miller, D. O., Meinardi, S., Li, Q., Lamarque, J. F., Kupc, A., Kjaergaard, H. G., Kinnison, D., Jimenez, J. L., Jernigan, C. M., Hornbrook, R. S., Hills, A., Dollner, M., Day, D. A., Cuevas, C. A., Campuzano-  
1010 Jost, P., Burkholder, J., Bui, T. P., Brune, W. H., Brown, S. S., Brock, C. A., Bourgeois, I., Blake, D. R., Apel, E. C. and Ryerson, T. B.: Global airborne sampling reveals a previously unobserved dimethyl sulfide oxidation mechanism in the marine atmosphere, *Proc. Natl. Acad. Sci. U. S. A.*, 117(9), 4505–4510, doi:10.1073/pnas.1919344117, 2020.
- Volkamer, R., Sheehy, P., Molina, L. T. and Molina, M. J.: Oxidative capacity of the Mexico City atmosphere-Part 1: A radical source perspective, *Atmos. Chem. Phys.*, 10(14), 6969–6991,  
1015 doi:10.5194/acp-10-6969-2010, 2010.
- Wang, L. and Zhang, J.: Detection of nitrous acid by cavity ring-down spectroscopy, *Environ. Sci. Technol.*, 34(19), 4221–4227, doi:10.1021/es0011055, 2000.
- 1020 Washenfelder, R. A., Roehl, C. M., McKinney, K. A., Julian, R. R. and Wennberg, P. O.: A compact, lightweight gas standards generator for permeation tubes, *Rev. Sci. Instrum.*, 74(6), 3151–3154, doi:10.1063/1.1570949, 2003.
- Ye, C., Zhou, X., Pu, D., Stutz, J., Festa, J., Spolaor, M., Tsai, C., Cantrell, C., Mauldin, R. L.,  
1025 Campos, T., Weinheimer, A., Hornbrook, R. S., Apel, E. C., Guenther, A., Kaser, L., Yuan, B., Karl, T., Haggerty, J., Hall, S., Ullmann, K., Smith, J. N., Ortega, J. and Knote, C.: Rapid cycling of reactive nitrogen in the marine boundary layer, *Nature*, 532(7600), 489–491, doi:10.1038/nature17195, 2016.
- 1030 Ye, C., Zhou, X., Pu, D., Stutz, J., Festa, J., Spolaor, M., Tsai, C., Cantrell, C., Mauldin III, R. L., Weinheimer, A., Hornbrook, R. S., Apel, E. C., Guenther, A., Kaser, L., Yuan, B., Karl, T., Haggerty, J., Hall, S., Ullmann, K., Smith, J. and Ortega, J.: Tropospheric HONO distribution and chemistry in the southeastern US, *Atmos. Chem. Phys.*, 18, 9107–9120, doi:10.5194/acp-2018-105, 2018.
- 1035 Young, C. J., Washenfelder, R. A., Roberts, J. M., Mielke, L. H., Osthoff, H. D., Tsai, C., Pikel'naya, O., Stutz, J., Veres, P. R., Cochran, A. K., Vandenboer, T. C., Flynn, J., Grossberg, N., Haman, C. L., Lefer, B., Stark, H., Graus, M., De Gouw, J., Gilman, J. B., Kuster, W. C. and  
1040 Brown, S. S.: Vertically resolved measurements of nighttime radical reservoirs in Los Angeles and their contribution to the urban radical budget, *Environ. Sci. Technol.*, 46(20), 10965–10973,

doi:10.1021/es302206a, 2012.

- 1045 Young, C. J., Zhou, S., Siegel, J. A. and Kahan, T. F.: Illuminating the dark side of indoor oxidants, *Environ. Sci. Process. Impacts*, 21(8), 1229–1239, doi:10.1039/c9em00111e, 2019.
- Zhang, N., Zhou, X., Shepson, P. B., Gao, H., Alaghmand, M. and Stirm, B.: Aircraft measurement of HONO vertical profiles over a forested region, *Geophys. Res. Lett.*, 36(15), L15820, doi:10.1029/2009GL038999, 2009.
- 1050 Zhang, W., Tong, S., Ge, M., An, J., Shi, Z., Hou, S., Xia, K., Qu, Y., Zhang, H., Chu, B., Sun, Y. and He, H.: Variations and sources of nitrous acid (HONO) during a severe pollution episode in Beijing in winter 2016, *Sci. Total Environ.*, 648, 253–262, doi:10.1016/j.scitotenv.2018.08.133, 2019.
- 1055 Zhou, S., Young, C. J., Vandenboer, T. C., Kowal, S. F. and Kahan, T. F.: Time-resolved measurements of nitric oxide, nitrogen dioxide, and nitrous acid in an occupied New York home, *Environ. Sci. Technol.*, 52(15), 8355–8364, doi:10.1021/acs.est.8b01792, 2018.
- 1060 Zhou, X., He, Y., Huang, G., Thornberry, T. D., Carroll, M. A. and Bertman, S. B.: Photochemical production of nitrous acid on glass sample manifold surface, *Geophys. Res. Lett.*, 29(14), 1681, doi:10.1029/2002gl015080, 2002.

1065 **Tables and Table Captions**

1070 **Table 1.** Description of custom-made HCl permeation devices used to generate HONO. Zero air-corrected mixing ratios of emitted HCl and generated HONO using a single NaNO<sub>2</sub>-coated PFA reaction device were measured with the heated Al-block at 40 °C in 1.1. SLPM. The variability reported for each observation represents one standard deviation from the mean (n = 30 to 60 using 1-minute averaged data).

| PD    | HCl (M) | Date of Manufacture (YYYY/MM) | PFA Device (cm) | PTFE Plug (cm) | HCl (ppbv) | HONO (ppbv) | Measured Date (YYYY/MM) |
|-------|---------|-------------------------------|-----------------|----------------|------------|-------------|-------------------------|
| PD-1  | 1.2     | 2017/04                       | 9.92            | 0.60           | 0.58 ±0.01 | 0.95 ±0.51  | 2019/10                 |
| PD-6a | 6       | 2017/04                       | 9.41            | 0.70           | 0.21 ±0.01 | 0.88 ±0.4   | 2019/10                 |
| PD-6b | 6       | 2019/04                       | 9.11            | 0.75           | 2.0 ±0.01  | 2.8 ±0.41   | 2019/11                 |
| PD-6c | 6       | 2019/04                       | 9.65            | 0.70           | 5.0 ±0.3   | 6.2 ±0.5    | 2019/11                 |

1075 **Table 2.** Mass balance of measured mixing ratios of HCl entering and HONO exiting the calibration source to determine acid displacement efficiency (ADE) at 50 % RH and 40 °C. Uncertainties represent 1σ standard deviation from the mean for ≥30 min of measurements and 1σ propagated error for calculated values.

| PD    | HCl <sub>IN</sub> (ppbv) | HONO from HCl+H <sub>2</sub> O (ppbv) | HONO from H <sub>2</sub> O (ppbv) | HONO from H <sub>2</sub> O (%) | ADE (%) |
|-------|--------------------------|---------------------------------------|-----------------------------------|--------------------------------|---------|
| PD-6a | 0.08 ±0.002              | 0.31 ±0.15                            | 0.24 ±0.14                        | 77 ±45                         | >99     |
| PD-6b | 2.2 ±0.011               | 2.78 ±0.41                            | 0.61 ±0.44                        | 22 ±16                         | >99     |

1080 **Table 3.** Average mixing ratios of HCl input (PD-6a), and HONO emitted from reaction with water vapour and with both reagents as function of temperature. Uncertainty denotes 1σ standard deviation from the mean of measured values.

| Temperature (°C) | HCl (ppbv)   | HONO from H <sub>2</sub> O (ppbv) | Total HONO (ppbv) |
|------------------|--------------|-----------------------------------|-------------------|
| 30               | 0.230 ±0.003 | 0.3                               | 0.5 ±0.4          |
| 40               | 0.330 ±0.007 | 0.7                               | 1.0 ±0.5          |
| 50               | 0.660 ±0.037 | 1.3                               | 2.0 ±0.5          |

**Table 4.** Average measured HONO mixing ratios (ppbv) using different ½” inner diameter tubing. All results at 40 °C and using same HCl PD (PD-6c). Variability shown is 1σ from the mean.

| Device material | HONO (ppbv) |
|-----------------|-------------|
| PFA             | 6.20 ±0.50  |
| Etched PFA      | 5.68 ±0.71  |

|                 |            |
|-----------------|------------|
| Stainless Steel | 6.75 ±0.83 |
| Nylon           | 6.06 ±0.61 |
| Quartz          | 3.72 ±0.55 |

1085 **Figure Captions**

**Figure 1.** Flow and component schematic of the HONO calibration system (pink shaded region) interfaced with a NO<sub>x</sub> analyzer (green), dilution mass flow controller (blue), and an exchangeable Na<sub>2</sub>CO<sub>3</sub> annular denuder (yellow). Lines with black arrows denote the direction of gas flow through system components. Tee and cross fittings are denoted by arrays of grey triangles.

**Figure 2.** Conversion efficiency of HCl (blue) to HONO (red) via the acid displacement reaction on a NaNO<sub>2</sub> reaction device. The HCl PD-6a and one coated PFA device were used and measured following two hours of stabilization. The acids were observed by acetate quadrupole CIMS with time resolution of 0.50 s and averaged to 60 s. Yellow shaded regions indicate the addition of zero air to the instrument inlet for background correction, while red and blue shaded regions correspond to 1σ variance in the observations. Note that the variance in the HCl trace is similar to the width of the line.

**Figure 3.** Mixing ratios of HONO observed using HCl PD-6a and three different, but freshly coated, NaNO<sub>2</sub> PFA reaction devices. Time zero indicates the start of HONO production in the calibration unit where no prior flow through the calibration unit existed, but all temperatures were stable at 40 °C. The vertical dashed line denotes the time where the output of the three devices are no longer statistically different from each other. Reported measurements are one-minute average data with a 30 s Kalman filter on the NO<sub>x</sub> analyzer.

**Figure 4.** (a) CRDS high-resolution observation an HCl emission pulse (red) and H<sub>2</sub>O decrease (blue) from PD-6a resulting in 50 % increase of the HCl mixing ratio emitted. (b) Time series of four consecutive measurement periods of HONO production, using only PD-6c and a new NaNO<sub>2</sub> coated reaction device in each run. (c) Box (1<sup>st</sup> and 3<sup>rd</sup> quartile) and whiskers (3σ from the mean) of HONO mixing ratios observed for the four runs are binned by duration of use for each new reaction device in hours. Mean values are indicated with a filled dark blue diamond marker, median values by the light blue crossed box marker, dark pink circles are 2σ outliers and dark red squares 3σ outliers.

**Figure 5.** (a) Mixing ratios of HONO for the eight field transport simulations (FS, Table S1). All observations were background corrected by linear interpolation across the experiments using zero air before and after HONO observations and an Na<sub>2</sub>CO<sub>3</sub> coated annular during (Fig. S4). (b) Box and whiskers plot of the HONO output using measurements collected after two hours of calibration source stabilization. The light blue crossed box represents the median, the dark blue diamond the mean, light pink circles the data points, dark pink circles the 3σ outliers, and the black box the 1<sup>st</sup> and 3<sup>rd</sup> quartiles of observed HONO mixing ratios. The whiskers denote the 3σ standard deviation.

1120 **Figure 6.** Mixing ratio of HONO produced from a NaNO<sub>2</sub> coated annular denuder using PD-6c. Time zero is when HCl was first introduced to the annular denuder at 50 % RH. Note that HONO mixing ratios are on a log scale.